Acta Acustica 2024, **8**, 53
© The Author(s), Published by EDP Sciences, 2024
https://doi.org/10.1051/aacus/2024045

Topical Issue – Musical Acoustics: Latest Advances in Analytical, Numerical and Experimental Methods Tackling Complex Phenomena in Musical Instruments

Available online at:
https://acta-acustica.edpsciences.org

SCIENTIFIC ARTICLE

OPEN ACCESS

Affordable wide-band measurement ecosystem for musical acoustics based on electro-dynamic transducers

Ludovico Ausiello[1,*], Michele Ducceschi[2], Sebastian Duran[2], and Benjamin Morrison[1]

[1] School of Electrical and Mechanical Engineering, University of Portsmouth, Anglesea Rd, PO1 3DJ, Portsmouth, Hampshire, UK
[2] Department of Industrial Engineering, University of Bologna, Viale del Risorgimento 2, 40136 Bologna, Italy

Received 8 December 2023, Accepted 25 July 2024

Abstract – The variability in responses of acoustic instruments can be attributed to a combination of fluctuations in critical parameters of wood, such as density, stiffness, and strength, and design features such as body shapes or bracing geometries. Recent studies have successfully implemented the sine sweep method with small exciters to measure the acoustic response of guitars, yielding frequency responses with high coherence over a bandwidth reaching up to 8 kHz. This paper proposes validating a cost-effective measurement system which integrates electro-dynamic transducers and wide-band test signals (sine sweep and noise) against the traditional impact hammer method in the case of unbraced plates. Data from four actuators of different size and power will be presented together with a simple strategy to assess reliable and neutral excitation points, thanks to two complementary models which describe the interaction between exciter and plate. The paper will then showcase the applications of this measurement system in two scenarios. The first case study will focus on a cost-effective method for selecting acoustic wood, while the second will explore experimental real-time spectral analysis using pink noise. These case studies demonstrate the measurement system's adaptability and immediacy, providing valuable insights for enhancing the design and performance of acoustic instruments.

Keywords: Acoustic measurements, Musical acoustics, Exponential sine-sweep, Soundboards, Exciter, Impedance measurements

1 Introduction

While electrical and acoustic measurements are standardised practice to monitor the production in the loudspeaker and microphone industry and market [1–3], data representing the acoustic response of commercial acoustic musical instruments is seldom provided. The diversity in the response of acoustic instruments is related to variations of key parameters of wood, such as density, stiffness, and strength, as well as design features, such as body shapes, the thickness of components, etc. This is well documented [4, 5], with specific data regarding spruce [6–8], the most widely used wood type for soundboards [9–11]. Concerning guitars, numerical models have proved to be a powerful tool in investigating the impact of material properties, climatic conditions, bracing patterns, and body shapes on the instrument acoustics' performance [12–14]. Recent findings suggest that, within the response of a classical guitar, some specific modes are highly sensitive to the variations of material parameters. In contrast, others depend more on the braces' geometry and height [4]. Also, data-driven studies on violins report that response similarity can be achieved by selecting wood properties or by altering the shapes and thickness of top plates [5]. Interpreting these results is not straightforward. Experimental modal analysis techniques could be a viable option to certify the acoustic signature of a finalised design or sub-assembly [15]. Still, there is a lack of simple and low-cost solutions to measure and implement a desirable response from an acoustic instrument or its main components, such as a soundboard.

Recent pilot studies [16, 17] successfully employed the sine sweep method to gather the acoustic response of a guitar using small exciters. Sine sweeps yield large frequency bandwidth measurements with high coherence values between the applied force and the corresponding vibrational or acoustic output of the Device Under Test (DUT) [16, 18, 19]. The intrinsic repeatability and good accuracy of the method are paired with a low-cost setup consisting of electro-dynamic exciters, accelerometers or pressure microphones (if an anechoic environment is available). These favourable properties suggest that the sine sweep method could be employed in various measurement stations along the production line to follow the evolution of a musical instrument (or their sub-assemblies and components) during construction [12, 14]. The presented work expands on the validation of the use of small exciters drawing from

*Corresponding author: ludovico.ausiello@port.ac.uk

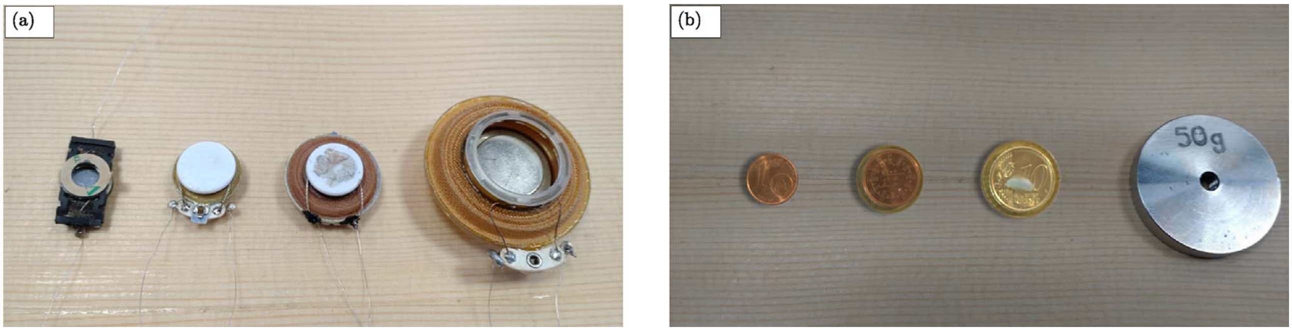

Figure 1. (a): The electro-dynamic exciters used in this work (from left to right side: Exciter 1, 2, 3, 4). (b): equivalent masses (from left to right: 2.5 g, 6.5 g, 12.5 g, 50 g).

previous studies [20, 21], and applying the method to assess design characteristics of acoustic guitars [12, 14], with a focus on using wide-band excitation signals: sine sweeps and pink noise. The aim is to assess the feasibility of using small electro-dynamic exciters when performing acoustic analysis to aid the building process. This paper is organised as follows: Section 2 presents a validation of the sine sweep and small exciters method against the impact hammer. A reference unbraced board will be measured with an impact hammer and four electro-dynamic exciters of varying nominal power and size. In the same section, the influence of the exciter's position and electro-mechanical properties are addressed. Section 3 contains two case studies: Section 3.1 details a cost-effective measurement chain to select and rework six guitar soundboard prototypes according to an arbitrarily simplified acoustic target. Section 3.2 shows a second application involving a wide-band, continuous signal driving the exciters for real-time spectral analysis. A discussion of the presented results is given in Section 4.

2 Small exciters for musical acoustics measurements

The impact hammer method is a common technique for experimental modal analysis [22–25]. The impulse response (IR) is obtained by hitting the DUT with the tip of the hammer and recording the output using a contact sensor (accelerometer), a vibrometer, or a microphone. The short impact is an experimental approximation of a Dirac delta, and finite-width effects result in a progressive loss of energy in the mid-to-high frequency range [26]. Further constraints on the material used for the hammer's tip might also affect the usable range, especially when softwood such as spruce is involved [27]. The sine sweep method, on the other hand, offers a larger frequency bandwidth [18, 19]. Uses of this techniques are prominent in room acoustics [28–30] due to its resilience to background noise and to the ability to separate the nonlinear harmonic distortion from the linear part of the spectrum. This latter feature allows using sources with a significant input gain exciting high-frequency modes. In [16], an application of this technique to the measurement of an acoustic guitar is presented, and in [17], it is shown that this approach is capable of capturing changes such as the presence or absence of the varnish on the guitar top, and alterations in bracing patterns in both the soundboard and the back of the instrument.

Previous works suggest that using exciters or shakers for IR measurement in musical instruments [15, 25, 31] may affect the IR itself, so it is essential to specify what type of actuators are used for the investigation presented here. In [25], a setar with a small board surface of about 215 cm^2 was excited with a 500 g, B&K device. The large exciter's mass proved to have a severe impact on the gathered data. In [16, 17, 32], as well as for this investigation, much larger and heavier boards are considered (the area being 1200 cm^2, and the total mass ranging between 190 g and 200 g).

The four exciters chosen in this work have a total mass of approximately 2.5 g, 6.5 g, 12.5 g, and 50 g, as per Figure 1, including the wax or putty material used to position them on the plates. A benchmark measurement using the impact hammer technique will now be presented to assess the potential effects of an additional mass-spring system attached to an unbraced board. Additionally, electrical impedance measurements will be performed in two different excitation points, to help interpret the measurement across frequency ranges.

2.1 Effects of small exciters on the acoustic response of raw, unbraced boards

An unbraced, raw spruce board of dimensions 600 mm × 210 mm (length × width), and 4 mm thick, is considered in this experiment. The thickness of the board was measured on a matrix of 9 points using a gauge. Three measurements, equally spaced along the length (i.e., aligned to the spruce's grain), were repeated on the plate's left edge, the centre line, and the right edge. The resulting 9 values were averaged, and the error was kept to the decimal point. Accordingly, a stated thickness of 4 mm corresponds to 4 mm ± 0.1 mm (this will be used throughout the paper). The frame used, visible in Figure 2, is made of hard plexiglass, with a rectangular opening at the bottom not to impede vibration and a rectangular frame at the top to distribute the pressure provided by regularly spaced clamps evenly. The mass of the bottom structure is 5.650 kg, while the one for the top rectangular bezel is about 380 g, for a

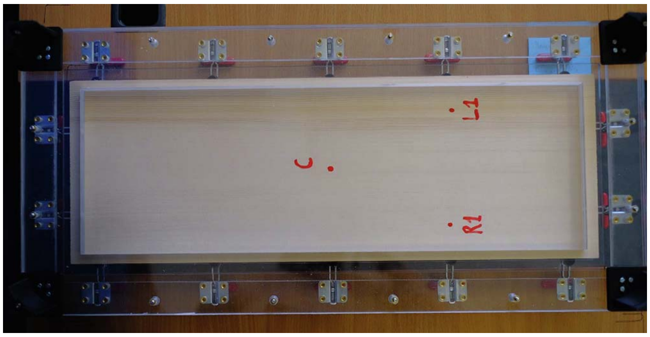

Figure 2. Schematic representation of the measurement setup. The red dots L1 and C indicate the excitation points, namely locations for either the impact hammer hits or the contact point for the exciters while performing the validation measurements, while R1 indicates the position of the accelerometer.

total mass of more than 6 kg. In Figure 2, L1 and C indicate the locations of the excitation points, while R1 is the position where the accelerometer was glued on the top surface of the DUT. Such locations on the board were chosen to minimise or maximise the impact of the actuators on the board, as will be discussed shortly.

The reference impact hammer is a miniature model PCB Piezotronics 086E80, while the accelerometer is a PCB Piezotronics 352C23 model. The exciters used in this experiment are four small electro-dynamic actuators named EXC_1, EXC_2, EXC_3, and EXC_4, characterised by the Thiele and Small (T&S) parameters [33–35] in Table 1. Their dimensions are progressively larger, as well as their *Bl* and force factor (where *l* denotes the length of the conductor immersed in the magnetic flux density *B*), indicating a larger power handling capability and a higher efficiency in exciting the board. The actuators' T&S parameters were measured using the "added-mass" method [36].

2.1.1 Assessing the added exciter's mass

One obvious question concerns the effect of the exciter's added mass on the collected IR. For each exciter, four configurations were used to assess this issue: first, the impact hammer technique was used on the raw board; second, the same impact hammer technique was used on the board augmented with a coin the same weight as the exciter; third, the impact hammer technique was used on the board augmented with the exciter; fourth, the exciter and sine sweep method was used.

The excitation point L1 was considered first, with the accelerometer placed in R1 all the while. To collect reliable data, the miniature impact hammer measurements were averaged across five repetitions [16, 22]. Note that all impact hammer measurements throughout the paper were subjected to the same averaging procedure, but this will not be stated further for brevity. The hammer and accelerometer signals were read by a Zoom F8 audio interface, connected to Audacity to record multiple hits regularly spaced in time. The coins have masses of 2.5 g, 6.5 g, 12.5 g, and 50 g, the same as the four exciters as per Table 1. The signal chain driving the exciters consisted of a laptop with Adobe Audition 3.0 generating a (45–8000) Hz sine sweep stimulus normalised at −6 dB LUFS, which was outputted by a Focusrite Scarlet 2i2 audio interface into a 20 W linear amplifier. Each stimulus contained two sweeps, ten seconds long, with a silence interval of 5 s in between. For all measurements, the sampling frequency was 48 kHz and the bit-depth was 24 bit [19]. The stimulus output voltage measured at the exciters' terminals was calibrated depending on the nominal impedance of each actuator to produce 0.25 W of power at 1 kHz. This was measured by a Fluke 177 multimeter at the exciter's terminals.

Frequency response functions (FRF) were computed by dividing the cross-power spectrum of the input and output measurement signals by the autopower spectrum of the input force of the hammer signal. The spectra are plotted in terms of the mobility *Y* in dB. Results of the four experiments are collected in Figure 3, where the benchmark FRF gathered using the impact hammer is displayed as a solid blue line. The coin-mass and exciter-mass cases are shown in green and red, respectively, while the black solid curve represents the FRF acquired with the exponential sine sweep method. The results suggest that EXC_1 does not provide enough power to fully drive the first resonance of the DUT at low frequencies. This was expected, considering the device's *Bl* and T&S parameters. A good match is observed between the impact hammer curves, the exciter-mass case and the sine sweep case. Discrepancies are visible on the coin-mass case. Table 2 summarises the estimation relative error when using either the impact hammer or any of the four exciters in position L1.

The validation procedure was conducted similarly with excitation point C. This point was selected to maximise the differences across the various measurement setups since it presents alternating nodes and antinodes for the modal shapes under clamped boundary conditions. Figure 4 illustrates the magnitude of the gathered FRFs in dB. The presence of the transducers significantly affects the results in the lower range. Discrepancies are also evident between the coin-mass and exciter-mass cases. The coin behaves as a passive added mass, shifting frequencies downward. Conversely, the presence of the exciters causes an upward shift, suggesting a different behaviour, now discussed.

2.1.2 Assessing the exciters' impedance

Electrical impedance measurements are employed in loudspeaker design to evaluate the self-resonant behaviour of the mass-spring system comprising the voice coil, spider, surround, and the vibrating membrane [33, 35, 37, 38], and were repeated here to investigate the coupling between the board's response and the mechanical part of the driver. A Clio Pocket system by Audiomatica[1] was used for the impedance measurements. It comes calibrated from the factory and performs absolute readings, which are then exported and processed in Matlab. It consists of a USB external acquisition unit with one input and one output channel. For the investigation, the output channel was used in

[1] Audiomatica, https://www.audiomatica.com/wp/?page_id=3557

Table 1. Thiele and Small (T&S) parameters of the four exciters, measured in free air.

	Total Mass (g)	f_{md} (Hz)	R_{e} (Ω)	Q_{ms}	Q_{es}	Q_{ts}	C_{ms} (mmN^{-1})	M_{ms} (g)	R_{ms} (Ωm)	Bl (NA^{-1})	L_{e} (mH)
EXC_1	2.5	1325	3.5	24.72	445.3	23.42	0.14	0.10	0.03	0.08	0.01
EXC_2	6.5	483	7.0	12.43	11.9	6.09	0.20	0.52	0.13	0.97	0.04
EXC_3	12.5	454	1.7	7.90	2.80	2.07	0.20	0.58	0.21	1.01	0.02
EXC_4	50	333	4.0	8.60	1.44	1.24	0.21	1.06	0.26	2.48	0.04

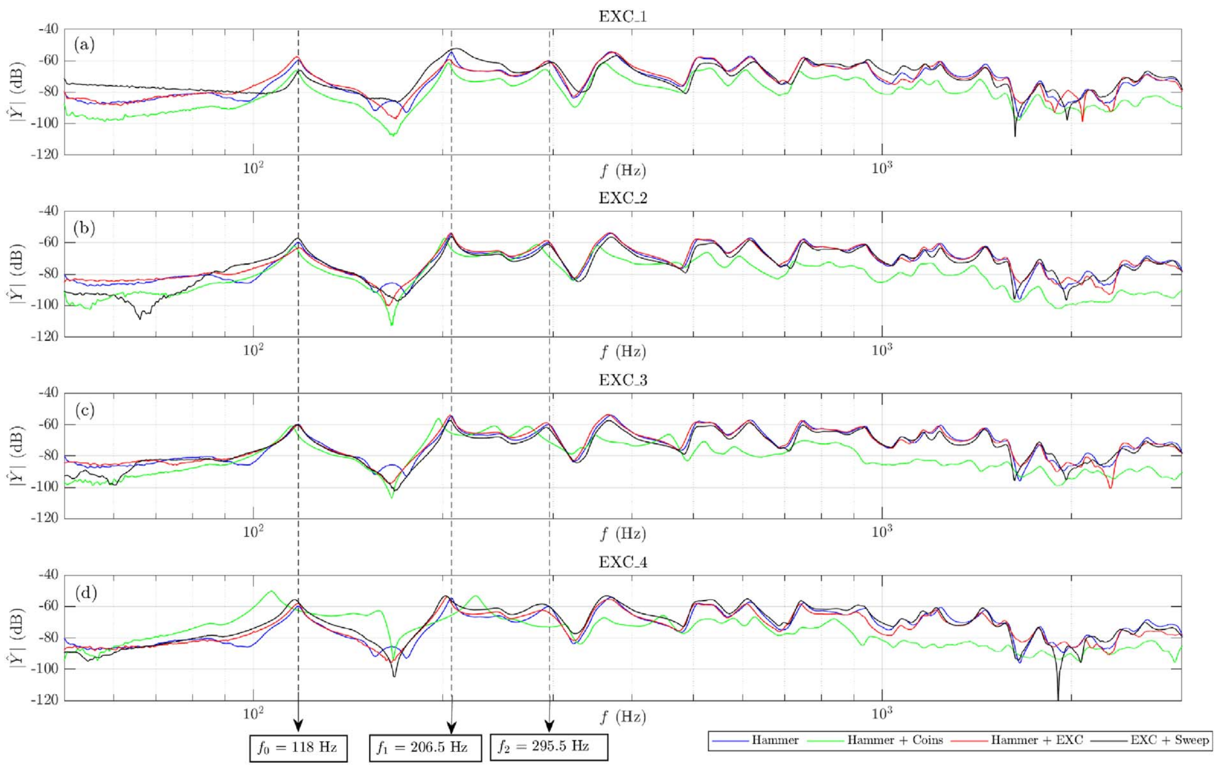

Figure 3. Exciter validation. For all panels, the spectra are as follows: hammer on raw board (solid blue); hammer on board plus exciter (red); hammer on board plus coin (green); sine sweep and exciter (black). The coins have the same mass as the exciters, as per Table 1. Input point in L1, readout in R1.

Table 2. Frequency and relative deviations of first detected peak f_0 in the FRF spectra using the benchmark hammer measurement and the exciters. The excitation point is L1.

Hammer	f_0 (Hz)	EXC_1 118.5	EXC_2 117.5	EXC_3 117	EXC_4 116
$f_0 = 118$ Hz	dev. (%)	0.42	−0.43	−0.85	−1.72
	dev. (cent)	7	−7	−14	−29

closed-loop to measure the impedance, $|Z|$, by outputting a known voltage and simultaneously measuring a current through an internal reference resistor and the transducer [36]. The latter was connected via a cable terminating with crocodile clips, which showed an internal resistance of 0.1 $\Omega \pm 0.05$ Ω. The actuators were wired using thin, light, and flexible wires. When an exciter was mounted on the board, its wires were bonded to the plexiglass frame visible in Figure 2 with putty. A portion of each wire created a small arc, while the remaining portion after the putty was attached to a crocodile clip.

A preliminary statistical analysis measured EXC_3 in position L1 32 times. The actuator was re-positioned on the board several times (using the same amount of wax). At the same time, small variations on its location or orientation were introduced to mimic a real-life scenario. The analysis showed that the single large impedance peak was located, on average, at 75.6 Hz ± 2.7 Hz with a mean amplitude of 3.76 $\Omega \pm 0.57$ Ω. EXC_1 was excluded from the study due to its limited performance. The remaining three actuators were measured, and their impedance curves were recorded while located in both positions L1 and C, similar to the configurations used to capture the IR of the soundboard. Figure 5 compares the two excitation points. Furthermore, a second experiment was designed to highlight the effects of adding mass to the exciters in both excitation points. Figure 6 shows the results for EXC_3.

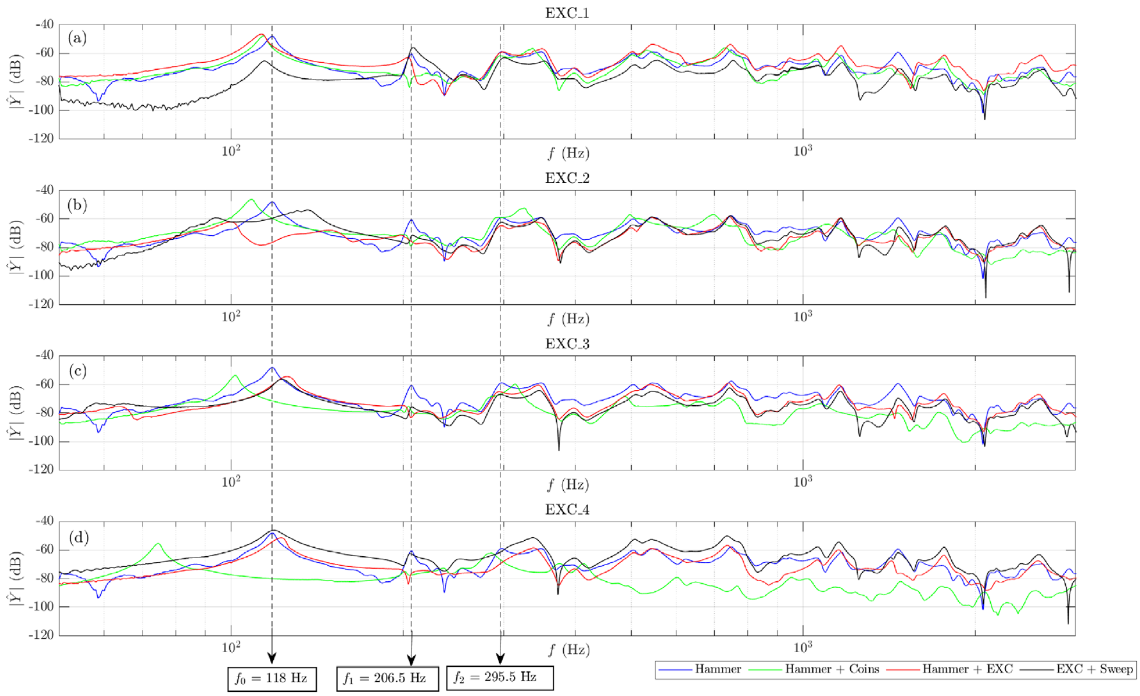

Figure 4. Exciter validation. Same as Figure 3, but excitation point in C.

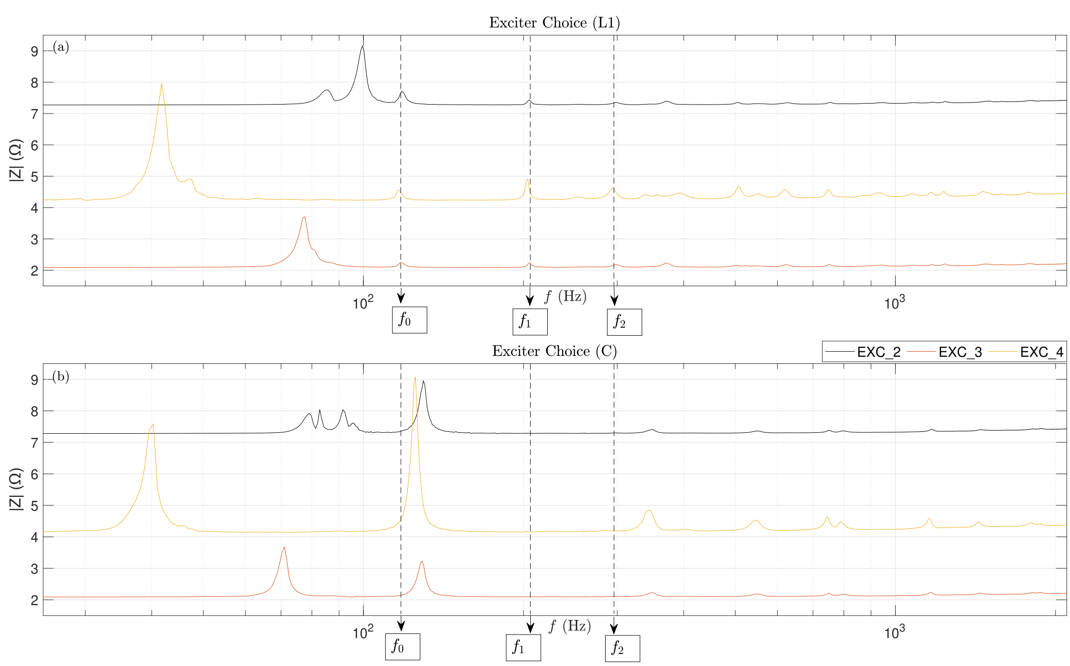

Figure 5. Electrical impedance plots of three exciters placed in L1 (panel (a)) and C (panel (b)). The dashed lines represent the first resonances of the board. In position L1, all curves present a single large peak followed by small local maxima. In position C, all curves show two large peaks and a different set of local maxima.

2.1.3 Modelling the electromechanical coupling

The experimental results can be understood by modelling the coupling between the board and the exciter. The coupled system is given as:

$$\rho h \frac{\partial^2 u(\mathbf{x},t)}{\partial t^2} = \mathcal{L}(u(\mathbf{x},t)) - 2\sigma\rho h \frac{\partial u(\mathbf{x},t)}{\partial t} + \delta(\mathbf{x}-\mathbf{x}_{\mathrm{md}})C_{\mathrm{ms}}(w(t) - u(\mathbf{x}_{\mathrm{md}},t)) - \delta(\mathbf{x}-\mathbf{x}_{\mathrm{md}})BlI(t) \tag{1a}$$

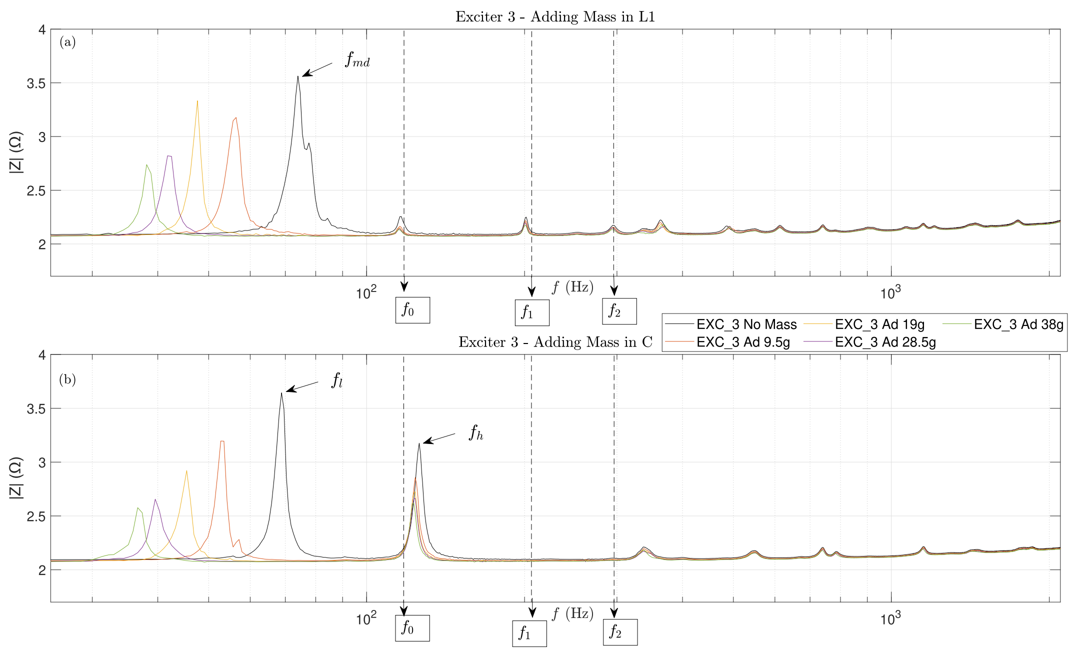

Figure 6. Electrical impedance plots of EXC_3 placed in L1, panel (a), and C, panel (b). Rigid masses are progressively added on the exciter to alter its mechanical resonance (f_{md}). The dashed lines represent the first modes of the board; mode (0, 0) ($f_0 = 118$ Hz) is located near the first small local maxima in panel (a), and in between the peaks f_l and f_h ("low" and "high") in panel (b). A good excitation point (a) can be identified when a single peak f_{md} (resonance of DUT + transducer) is visible. When mass is added, f_{md} shifts down in frequency, while smaller local maxima of the curve are not affected.

$$M_{\mathrm{ms}}\ddot{w}(t) = -2M_{\mathrm{ms}}\eta\dot{w}(t) - C_{\mathrm{ms}}(w(t) - u(\mathbf{x}_{\mathrm{md}}, t)) + BlI(t) \tag{1b}$$

$$V(t) = L_e\dot{I}(t) + R_eI(t) + K(\dot{w}(t) - \dot{u}(\mathbf{x}_{\mathrm{md}}, t)). \tag{1c}$$

In the above, $u = u(\mathbf{x}, t)$ is the displacement of the board, for coordinate $\mathbf{x} \in (0, L_x) \times (0, L_y)$ and time t; $w = w(t)$ is the displacement of the exciter. $I = I(t)$ is the current through the exciter, and $V(t)$ is the externally-supplied voltage.

In (1a), $\mathcal{L}(u)$ represents the differential operator associated with the orthotropic plate equation, not specified here for brevity. See e.g. [39] for an explicit form of such operator. Furthermore, in the above, $\mathbf{x}_{\mathrm{md}}$ denotes the coordinate of the exciter's contact point on the board, which may be identified as C or L1.

Constants appear as: $\rho = 390$ kg · m^{-3}, the density of the board; $h = 4$ mm, its thickness. Furthermore, M_{ms}, C_{ms}, R_{e}, L_{e}, Bl are the Thiele & Small paramters of the exciter when attached to the board, and are summarised in Table 3. Finally, σ, η and K are, respectively, the loss coefficient of the board, the loss coefficient of the exciter when attached to the board, and a constant of back-electromechanical coupling. For brevity, only EXC_3 will be considered here. It is convenient to derive a reduced-order model (ROM) comprising the plate's first mode alone since this is the most influenced by the location of the exciter $\mathbf{x}_{\mathrm{md}}$. To that end, for the sake of simplicity, it is assumed that

$$u(\mathbf{x}, t) \approx \sin\frac{\pi x}{L_x}\sin\frac{\pi y}{L_y}q(t), \tag{2}$$

where the modal shape given here corresponds to the first mode of a simply-supported board, and where $q(t)$ represents the time evolution of the mode. The mathematical expression for the modal shape is justified as the first modal shape of the clamped board is "qualitatively" similar in that it presents a maximum at the plate's centre and progressively tapers off toward the edges. Inserting (4) in (1) and performing a standard modal projection [40] leads to the reduced order system:

$$\ddot{q}(t) = -\omega_0^2 q(t) - 2\sigma\dot{q}(t) + bM_{\mathrm{ms}}M^{-1}\,\omega_{\mathrm{md}}^2(w(t) - bq(t)) - bM^{-1}BlI(t) \tag{3a}$$

$$\ddot{w} = -2\eta\dot{w}(t) - \omega_{\mathrm{md}}^2(w(t) - bq(t)) + M_{\mathrm{ms}}^{-1}BlI(t) \tag{3b}$$

$$V(t) = L_e\dot{I}(t) + R_eI(t) + K(\dot{w}(t) - b\dot{q}(t)). \tag{3c}$$

In the above, the modal weight was introduced as $b := \sin\frac{\pi x_{\mathrm{md}}}{L_x}\sin\frac{\pi y_{\mathrm{md}}}{L_y}$, quantifying the influence of the mode shape at the contact point. All parameters in the ROM are known or can be estimated easily. In fact, $\omega_0 = 2\pi f_0$, where $f_0 = 117$ Hz is the measured frequency of mode (0, 0) as given in Table 2 for EXC_3; $\sigma = 3\log(10)\tau_{60}^{-1} \approx 14\,\mathrm{s}^{-1}$ is estimated from the board's approximate decay time for mode (0, 0) of $\tau_{60} \approx 0.5$ s, where τ_{60} is the time required for the energy to decay by 60 dB per mode [41]; the modal mass of the board for mode (0, 0) is $M = 0.25\rho hL_x L_y \approx 50$ g, as given by the modal projection; $\mathbf{x}_{\mathrm{md}} := (x_{\mathrm{e}}, y_{\mathrm{e}})$ is estimated from Figure 2. For C one may take $\mathbf{x}_{\mathrm{md}} := (0.5L_x, 0.5\,L_y)$, and for L1 $\mathbf{x}_{\mathrm{md}} := (0.7L_x, 0.9L_y)$.

Table 3. Thiele and Small (T&S) parameters of EXC_3 when located in position L1. This configuration can be interpreted as a driver in free-air as intended in the works from Thiele, Lazar and Kubota, and Magalotti [33, 34, 42, 43]. A noticeable difference is visible in the value of the moving mass M_{ms}.

	F_{md} (Hz)	R_{e} (Ω)	C_{ms} (mm N^{-1})	M_{ms} (g)	Bl (NA^{-1})	L_{e} (mH)
EXC_3	73.9	2.1	0.35	13.18	1.01	0.06

$\omega_{\mathrm{md}} = 2\pi f_{\mathrm{md}}$, where $f_{\mathrm{md}} := \sqrt{C_{\mathrm{ms}} M_{\mathrm{ms}}^{-1}}/2\pi = 73.9\,\mathrm{Hz}$ as given in Table 3. η and K are guessed. Here, the following are used: $\eta \approx 15\ \mathrm{s}^{-1}$ and $K \approx 0.6\ \mathrm{V\ s\ m}^{-1}$. Considering a harmonic input forcing $V(t) = \hat{V} e^{j\omega t}$, one can transform the above in the frequency domain, obtaining:

$$\mathbf{Z}(\omega)\hat{\mathbf{I}} = \hat{\mathbf{V}} \tag{4}$$

where $\hat{\mathbf{I}} = (j\omega\hat{q} := \hat{v}, j\omega\hat{w}, \hat{I})^T$ is the frequency domain current/velocity response; $\hat{\mathbf{V}} = (0, 0, 1)^T$ is the input vector. $\mathbf{Z}(\omega)$ is the 3×3 impedance matrix, not given here for brevity. From the matrix, one can easily get the frequency-domain expressions for the board's response $\hat{v}$ and the electrical impedance $Z := \hat{V}/\hat{I}$. Results are given in Figure 7, where an excellent match with the experimental results is found.

The model agrees qualitatively and quantitatively with what is observed in Figures 3–5. In particular, note that exciting the board in C yields a stiffening of the first modal frequency in the board's response and the peak shifts to the right, as seen in the experiments summarised in Figure 4. In the same way, the peaks in the impedance plots change. In particular, placing the exciter in C activates a peak in the transducer's impedance corresponding to the compliant first mode.

The same peak is almost completely cancelled when the device is positioned in L1. These results suggest that placing the exciter around a modal maximum may affect the reliability of the measurement procedure, as the actuator does not act as a dead mass but rather as a stiffening device. However, choosing an excitation point away from clear resonances allows obtaining reliable measurements of the board. Furthermore, this model suggests that electrical impedance measurements at the exciter's terminals can detect compliant board peaks, which may affect the reliability of the measurement method.

A complementary interpretation can be offered to explain the data modelled in (1), by referring to the work of Thiele [33, 34], Lazar and Kubota [42], and Magalotti et al. [43] on loudspeaker desing. When the exciter is placed in L1, the DUT + exciter can be considered equivalent to a loudspeaker in free air. Conversely, with the exciter placed in C, the DUT + exciter can be seen as analogous to a loudspeaker placed in a vented box, i.e. coupled with a Helmholtz resonator. The former yields an impedance curve showing a single peak f_{md} as per Figure 6a, while the latter produces data depicted in Figure 6b, where two main peaks, named f_l, and f_h, are visible, exactly as per Figure 5, p. 385 in [33]. In the same reference, between f_l and f_h, a minimum called f_b is also identified, corresponding to the resonant frequency of the Helmholtz resonator (the vented box, hence the subscript b) to which a transducer is coupled. In the suggested interpretation, the first resonant frequency of the board f_0 is the analogous of f_b. The relationship between these three impedance peaks and the resonant frequency of the loudspeaker in free-air f_{md} is presented in [34], equation (105), and is written as:

$$f_{\mathrm{md}} = \frac{f_l \cdot f_h}{f_0}. \tag{5}$$

The validity of the analogy can be verified numerically. From the black curve of Figure 6b showing the impedance measurement of EXC_3 with no added mass in C, $f_l = 69$ Hz, and $f_h = 126$ Hz can be retrieved. From Table 2, $f_0 = 117$ Hz can be taken, thus yielding:

$$f_{\mathrm{md}} = \frac{69 \cdot 126}{117} = 74.3\mathrm{Hz}. \tag{6}$$

which is in agreement with the data discussed previously. When, from measurement, the interaction between the transducer and the board appears negligible, it can be assumed that the actuator is correctly working past its mechanical resonance [44]. Small local maxima of the impedance curve may still be visible in the proximity of the eigenmodes of the DUT, as discussed in literature [44, 45].

2.1.4 Coherence measurements

The collected data enables an investigation into the coherence between input and output signals, allowing a comparison of the effectiveness of the sine sweep and impact hammer approaches. As evidenced in Figure 8 in the case of EXC_3, it is observed that both methods exhibit comparable levels of correlation below 200 Hz. However, the impact hammer method demonstrates slightly higher coherence values at lower frequencies than the smaller exciters EXC_1 and EXC_2 (not shown). This difference can be attributed to their lower power rating and limited maximum displacement. Both approaches exhibit similar coherence values over frequencies up to 2–3 kHz. Nevertheless, while coherence begins to decline at 3 kHz for the impact hammer, the sine sweep driven by the exciter maintains a consistent coherence value up to the maximum frequency of the test signal (8 kHz in the presented experiments). This feature is relevant when testing soundboards using wide-band signals, such as the case presented in Section 3.2. This feature may also prove beneficial in scenarios where the wide-band spectrum of a musical instrument is required or in evaluating small sub-assemblies

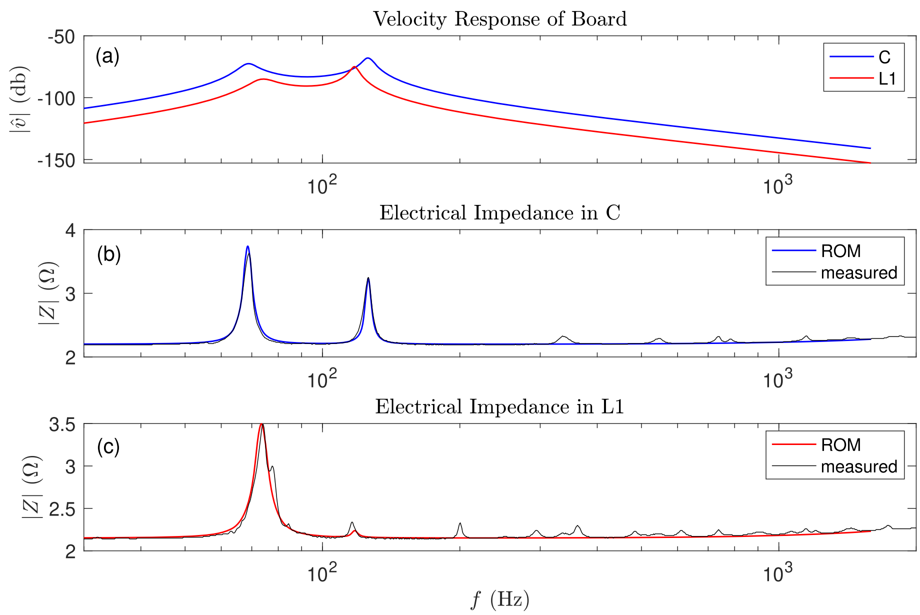

Figure 7. Reduced-order model (ROM) of the plate-exciter system for EXC_3. The stiffening of the system in position C is evident from the rightward shift of the board's resonance peak. The same peak is visible in the impedance plot, highlighting the increased mobility of the exciter when attached to the board.

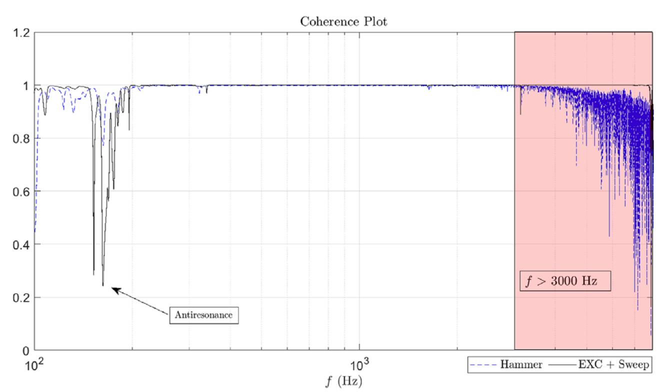

Figure 8. Coherence comparison between impact hammer method and sine sweep with EXC_3.

such as bridges and bows, where responses may extend to high frequencies.

3 Case studies

This section will elaborate on the use of small electrodynamic transducers in two specific applications. The first application involves employing sine sweep measurements to assess raw spruce boards upon receipt from a supplier. The second application employs pink noise and real-time spectral analysis to illustrate the ability to monitor changes in the vibrational response of a plate continuously, while adjusting a simplified bracing pattern in real-time. In accordance with previous findings, all measurements presented in Section 3.1 will employ excitation point L1.

3.1 Acoustic selection and simple tuning of spruce tops

An application of the sine sweep method driving EXC_4 for the purpose of soundboard selection is illustrated here. This experiment employed a selection of spruce soundboards of the same dimensions as the reference board described in Section 2, clamped in the same frame depicted in Figure 2. One Earthworks MD30 class-1 microphone was placed in the near-field of the vibrating soundboard, at 125 mm distance from the centre of the board, as per typical recording techniques [46, 47]. Similarly to Section 2, the output of EXC_4 was calibrated to 1 W at 1 kHz, and the recorded output from the DUT was processed with Adobe Audition and the Aurora plugins [19]. All spectral data presented was calculated with a 32768 samples-long discrete Fourier transform (DFT), leading to a frequency resolution of approximately 1.46 Hz.

The selection of raw spruce soundboards was supplied in the form of 12 quarter-sawn red spruce (Picea rubens) billets, which were already sawn in halves to produce what is called a *book-matched top*. The wood was bought from Ciresa[2] and was characterised by a tight specification on the density $\rho \in [380, 395]$ kg·m^{-3} $\pm$ 3 kg m^{-3}; three different aesthetic grades of spruce were available, i.e. type I, II, and III, sorted according to best quality in descending order, as per Table 4, where individual densities and identification numbers (ID) are also listed. As seen in Figure 9, data from the collected IRs indicate a large variation in the frequency of the fundamental mode of each set (f_0), with the parameter spanning the range $f_0 \in [104, 142]$ Hz. Inspection of the responses allowed to select a first group of three boards $\mathbf{S_1}$ = {"**125**", "**250**", "**346**"} sharing comparable

[2] Ciresa, https://www.ciresafiemme.it/en/

Table 4. Boards with corresponding quality type, density, initial f_0 before tuning, final f_0 after tuning, and final thickness values. Initial thickenss is $h^{\text{initial}} = 4$ mm for all boards. The boards' identifiers are marked with "ID" numbers, coming from the trees being cut to produce them. The blue rows include the boards belonging to group S_1, and the red rows include the boards belonging to S_2. The corresponding IDs are also highlighted in bold in the table.

Board "ID"	Quality	ρ (kg m^{-1})	f_0^{initial} (Hz)	f_0^{final} (Hz)	h^{final} (mm)
21	II	380	115	–	–
37	**II**	**381**	**134**	**104**	**3.15**
50	I	380	123	–	–
63	**III**	**380**	**130**	**106**	**2.8**
125	**III**	**394**	**122**	**117**	**3.5**
169	II	385	120	–	–
209	II	380	121	–	–
214	**II**	**390**	**104**	**104**	**3.9**
230	III	390	142	–	–
249	I	380	132	–	–
250	**II**	**388**	**123**	**117**	**3.4**
346	**I**	**389**	**126**	**117**	**3.4**

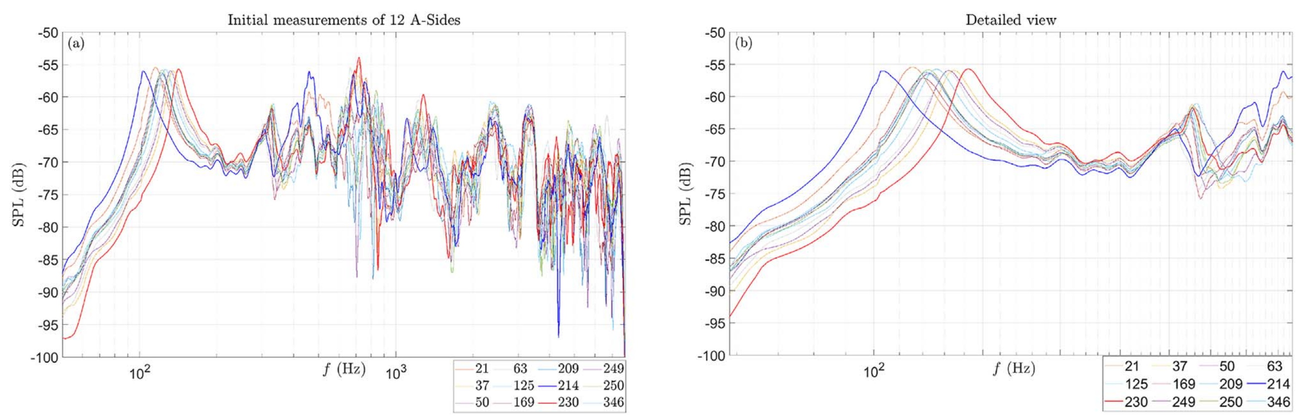

Figure 9. (a): Initial measurements of 12 A-Sides, exciter located at point L1, with 1/12th-octave smoothing applied. (b): Detailed view of the first resonance modes' frequencies. All boards and corresponding "IDs" are shown, suggesting the large variation of acoustic responses despite very similar material densities.

performance, despite the nominal difference in grain quality, as per Table 4. The initial fundamental frequencies for these are $f_0^{S_1} \in \{122, 123, 126\}$ Hz, respectively. A second group of three boards called $\mathbf{S_2} = \{$"**37**", "**63**", "**214**"$\}$ is selected for the opposite reason, that is, they presented a large variation for the fundamentals: $f_0^{S_2} \in \{134, 130, 104\}$ Hz, respectively.

Using a drum sander, boards of group S_1 and S_2 were gradually thinned to match an arbitrarily chosen acoustic target in terms of the frequency f_0 of the fundamental mode (0, 0), as suggested in [14]. The same 9-point thickness check was done as described in Section 2. After reworking specimens to a common value (e.g. 3.5 mm) the IRs were reassessed. The whole process was expected to lower the frequency of the first vibration mode since, according to plate theory, the frequency is proportional to the thickness. Group S_1 was the first one to be processed. The responses of the boards measured at $h = 4$ mm are shown in Figure 10a. When thickness equal to $h = 3.5$ mm was reached, board "125" showed a first resonance mode located at 117 Hz, while "250" and "346" were still resonating around (121–123) Hz. Accordingly, board "125" was left untouched, while the last two were machined again down to 3.4 mm, until the first mode of all three specimens is aligned at 117 Hz, see Figure 10b. Group S_2 was then processed. The responses of the half-boards measured at $h = 4$ mm are shown in Figure 11a. These plates were thinned down to h = 3.9 mm, at which board "214" still showed a first resonance at 104 Hz, while the other two resonated well above 126 Hz. These were finely machined in steps of 0.15 mm and measured. Eventually, board "37" was tuned at 104 Hz with a thickness of 3.15 mm, while board "63" showed a first resonance at 106 Hz despite being thinned down to 2.8 mm, see Figure 11b. Further thinning would compromise the structural integrity of the half-board, which was then left untouched. Figure 10b shows the

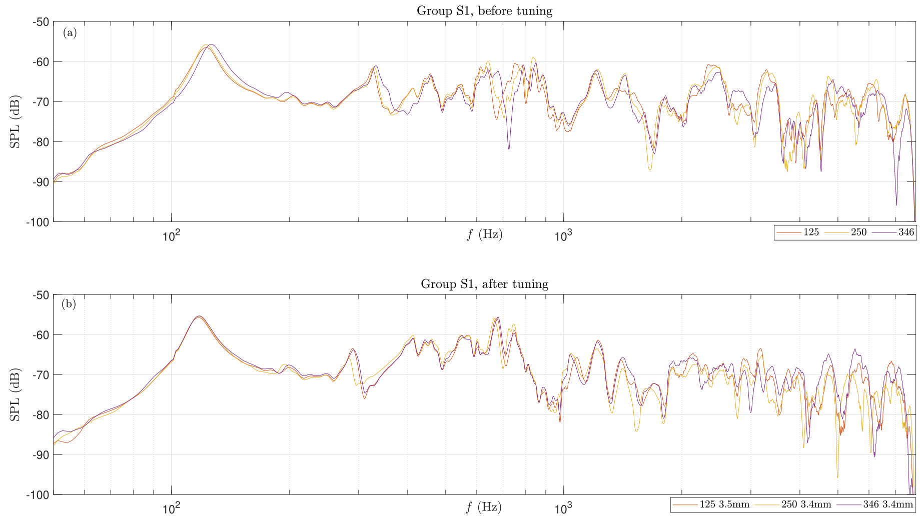

Figure 10. Tuning of boards S_1, corresponding "IDs" in the legend, with 1/12th-octave smoothing applied. (a): before tuning (all boards have thickness $h = 4$ mm). (b): after tuning to an arbitrarily chosen target for f_0 (boards have thicknesses as indicated). The results justify the use of exciters for affordable wide-band measurements.

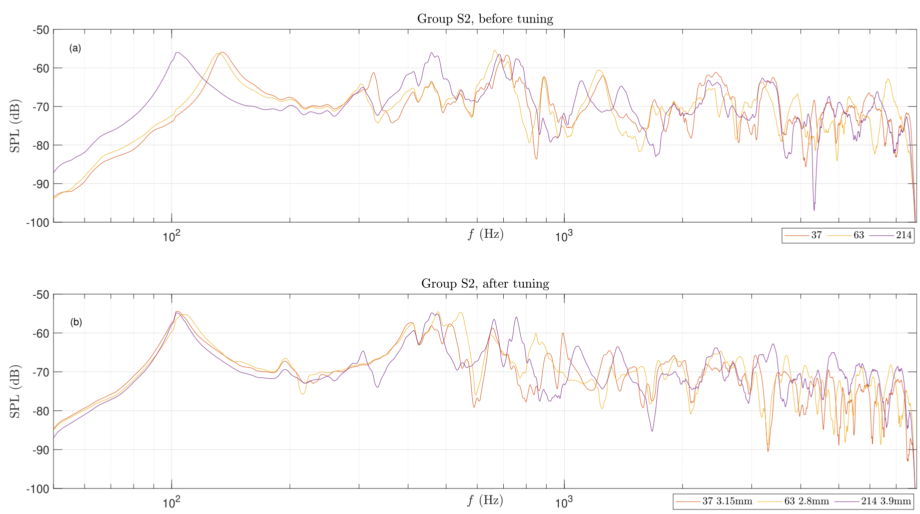

Figure 11. Tuning of boards S_2, corresponding "IDs" in the legend, with 1/12th-octave smoothing applied. (a): before tuning (all boards have thickness $h = 4$ mm). (b): after tuning to an arbitrarily chosen target for f_0 (boards have thicknesses as indicated).

wideband spectra of the reworked S_1 boards, displaying a good match up to 1 kHz and highlighting a practical application of the sine-sweep method.

3.2 Real-time spectral analysis of the response of a cantilever plate with moving braces

This case study used EXC_3. A small spruce board (300 mm × 160 mm × 3 mm) fixed in a cantilever constraint and positioned vertically was used in this experiment, as depicted in Figure 12.

Visible in the image are two small moving braces which were designed for this experiment. One is made out of quarter-sawn spruce, with density equal to 390 kg m^{-3} ± 3 kg m^{-3} and dimensions equal to 40 mm × 8 mm × 8 mm. The grain is aligned to the longitudinal direction of the braces and perpendicular to the board underneath. Flushed to the surface of the brace, 2 holes of 4 mm diameters are bored to host small N42 neodymium magnets of 4 mm diameter and 4 mm height. Accordingly, when the wooden brace was placed on the cantilever board, 1 additional N42 cubic magnet of 5 mm side was positioned on the other side of the plate to hold it in place, for a total number of 3 magnets. All magnets' north poles point in the same direction, maximising the attraction between the brace and the counter-magnet. The total mass of the moving brace plus the counter-magnet was 14 g. This difference, although relevant, was nonetheless necessary to change the absolute position and angle of the roving brace. A second embodiment of a roving brace consisted of the same cubic N42

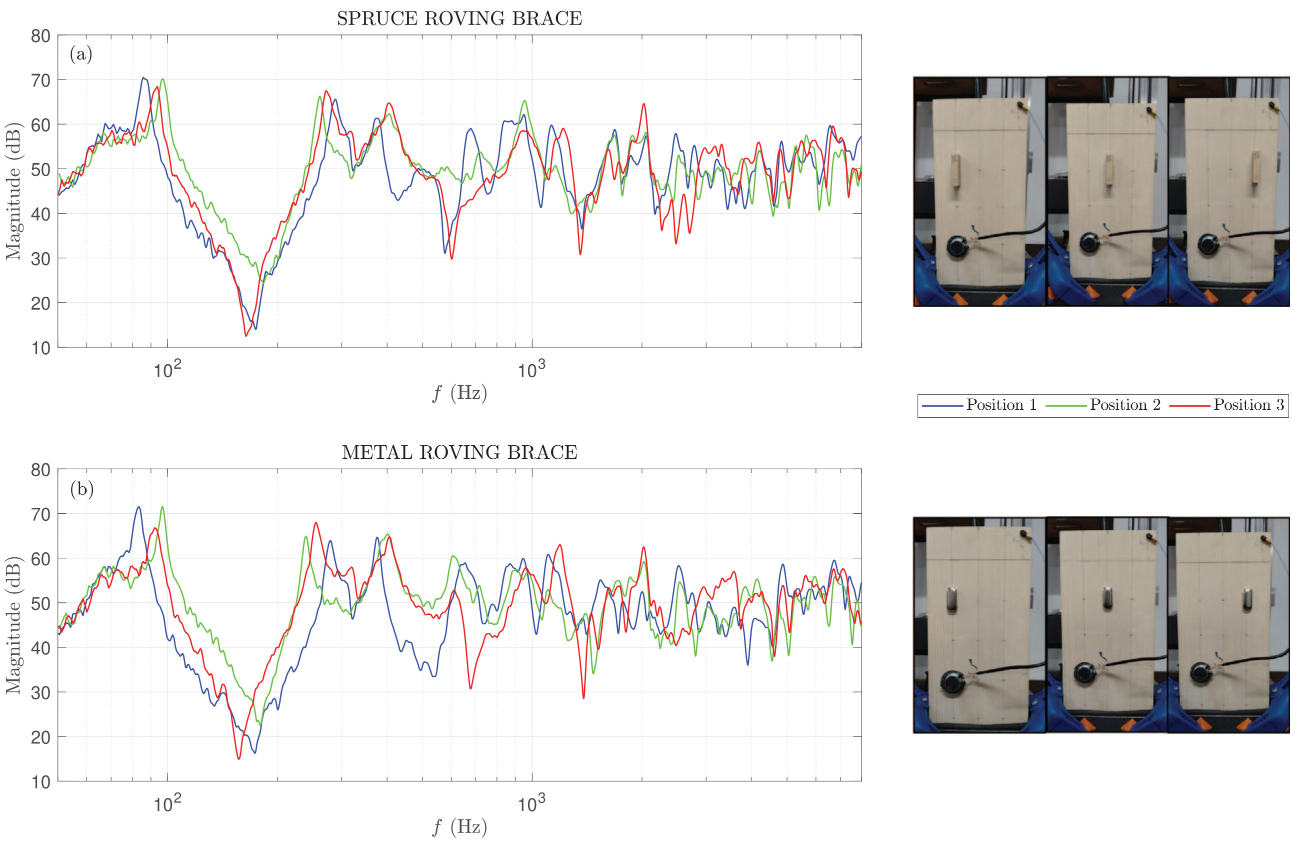

Figure 12. Snapshots of the real-time spectrum analysis, with 1/48th-octave smoothing applied, captured in position 1 (blue), 2 (green), and 3 (red), in the case of a spruce roving brace (a), or a metal roving brace (b).

magnet positioned on the back of the cantilever plate, attracting a small 1018 steel bar of 20 mm × 8 mm × 3 mm; the total additional mass of this second roving brace was 40 g.

The signal chain was calibrated to output 0.25 W of pink noise, as measured at the terminal of EXC_3 in free-air conditions. The actuator was attached with a thin layer of wax in the bottom corner of the cantilever, while a PCB Piezotronics 352C23 accelerometer was glued in the same way in the top corner of the plate (see Fig. 12). The sensor output was processed by the Zoom H8 audio interface, connected to a laptop running a real-time spectrum analyser implemented by REW 5.31. The spectrum was calculated using a 65536 samples-long window (Hann), with 50% overlap.

Two distinct experiments were conducted, employing both the spruce and the metal brace. These experiments involved the roving of the braces across three designated locations (labelled as positions 1, 2, and 3), as depicted in Figure 12. The real-time spectral analysis was recorded in two videos made accessible through the Supplementary materials. Within each predefined position, specific snapshots of the spectral data were captured. This methodology, adapted from techniques commonly used in loudspeaker measurements, was designed to assess the instantaneous effects of structural adjustments on the vibrational behaviour of the braced board.

4 Result analysis and comments

The use of small electro-dynamic actuators, driven by wide-band signals such as sine sweeps or pink noise, allows the acquisition of reliable data up to 8 kHz in frequency, as indicated by coherence analysis. This method was applied to guitar soundboards and is adaptable to other stringed instruments with a broader spectrum of fundamental frequencies, such as harpsichords and pianos. In a comparison test, three out of four low-cost transducers returned data matching the benchmark provided by the impact hammer technique using expensive equipment.

A robust method to identify an effective excitation point was explained based on impedance measurements, and two complementary models describing the coupling between an electro-dynamic transducer and an unbraced soundboard. This offered an effective methodology to select exciters with appropriate power handling capabilities, dimensions, and bandwidth. With as few as two electrical impedance measurements, users can verify the exciter's functionality beyond its mechanical resonance. Small local maxima in the impedance curve are expected near the eigenmodes of the DUT under such conditions.

In a first case study, the sine-sweep measurement was used to adjust the frequency of the first resonance mode (mode(0, 0)) of raw spruce billets to an arbitrary target. A group of boards labelled S_1 returned matching spectra up to 1 kHz after tuning. The overall cost of the experimental setup, which comprises one exciter, one condenser microphone, a standard audio interface, and freely available software, remains contained, making it an appealing option for small workshop operations. Findings related to group S_2 suggest that more sophisticated techniques are necessary for systematic optimization processes, although affordable measurement technology can be adjusted to account for such more specialised usage.

Implementing closed-loop real-time measurements using pink noise, as detailed in Section 3.2, represents a repeatable and time-saving alternative to the impact hammer technique. Integrating sine-sweep and pink noise analysis offers manufacturers novel methodologies for implementing practical optimization algorithms, whether in a luthier shop or for monitoring and archiving acoustic data evolution during instrument construction, from raw materials to final product.

5 Conclusions and future work

This study introduced an approach to assessing the spectral properties of guitar soundboards using small electro-dynamic actuators for wideband measurements. The results confirmed the reliability of the sine sweep method when compared to the conventional impact hammer technique, demonstrating its efficacy across a broad frequency bandwidth of up to 8 kHz. Moreover, the findings indicated that the sine sweep method, coupled with exciters of varying sizes, efficiently captured a wide range of acoustic responses, making it a versatile tool in musical instrument manufacturing.

Two complementary models were presented to explain the interaction between small exciters and an unbraced board, offering robust means to select an appropriate excitation point. Future work will expand on the electrical equivalent model of the presented setup, in order to extract more information from the DUT through electrical impedance measurements.

Two case studies exemplified the practical applications of this methodology. The first demonstrated a cost-effective approach to selecting and tuning spruce soundboards for guitars, aligning their fundamental resonance modes with desired acoustic targets. The data collected during the tuning process could be used to monitor the transformation of raw materials into sub-assemblies and for quality control. The second case study illustrated using pink noise and real-time spectral analysis. By dynamically adjusting the bracing patterns of a vibrating system, immediate feedback on the acoustic repercussions of structural modifications was provided. These applications highlight the potential of integrating such measurement techniques into production processes, offering a pragmatic avenue for achieving desired acoustic properties in musical instruments. Future research will explore the performance and reliability of low-cost piezoelectric sensors concerning the affordability of the measurement setup.

Acknowledgments

The authors wish to thank Mattia D'Antonio for his insight into the practical details of the impedance measurements of the exciters used for this research and Roberto Magalotti for his support in developing the lumped element model.

Funding

Michele Ducceschi and Sebastian Duran were supported by the European Research Council (ERC) under grant 2020-StG-950084-NEMUS.

Conflicts of interest

There is no conflict of interest for any of the authors of this article.

Data availability statement

All data presented and discussed in this paper are available from the corresponding author on request.

Supplementary material

Supplementary video is available at https://actaacustica.edp-sciences.org/10.1051/aacus/2024045/olm.
Video: Recordings of the real-time spectral analysis discussed in Section 3.2.

References

1. IEC: Sound system equipment – Part 21: acoustical (output-based) measurements. 60268-21, International Standard, 2018.
2. IEC: Sound system equipment – Part 4: microphones. 60268-4, International Standard, 2018.
3. AES: AES recommended practice for professional audio – Subjective evaluation of loudspeakers. 20-1996. AES Standard, 2008.
4. A. Brauchler, S. Gonzalez, M. Vierneisel, P. Ziegler, F. Antonacci, A. Sarti, P. Eberhard: Model-predicted geometry variations to compensate material variability in the design of classical guitars, Nature Scientific Reports 13 (2023) 12766.
5. S. Gonzalez, D. Salvi, D. Baeza, F. Antonacci, A. Sarti: A data-driven approach to violin making, Nature Scientific Reports 11 (2021) 9455.
6. A. Steffenrem, P. Saranpää, S. Lundqvist, T. Skrøppa: Variation in wood properties among five full-sib families of Norway spruce (*Picea abies*), Annals of Forest Science 64, 8 (2007) 799–806.
7. J.R. Moore, A.J. Lyon, G.J. Searles, S.A. Lehneke, D.J. Ridley-Ellis: Within- and between-stand variation in selected properties of sitka spruce sawn timber in the United Kingdom: implications for segregation and grade recovery, Annals of Forest Science 70 (2013) 403–415.
8. V. Gryc, P. Horácek: Variability in density of spruce (*Picea abies* [L.] Karst.) wood with the presence of reaction wood, Journal of Forest Science 53, 3 (2007) 129–137.
9. D. Boak, R. Johnston: Martin guitars: a technical reference, Hal Leonard Books, New York, 2009.
10. E. Whitford, D. Vinopal, D. Erlewine: Gibson's fabulous flat-top guitars, Backbeat, Lanham, Maryland, 2009.
11. T. Gore, G. Gilet: Contemporary acoustic guitar design and build, Trevor Gore, Australia, 2011.
12. R. Viala, V. Placet, S. Cogan: Model-based evidence of the dominance of the guitar brace design over material and climatic variability for dynamic behaviours, Applied Acoustics 182 (2021) 108275.
13. M. Boven: Dynamic response optimization of an acoustic guitar, PhD dissertation, TU Delft, Delft, Netherlands, 2017.

14. D. Salvi, S. Gonzalez, F. Antonacci, A. Sarti: Modal analysis of free archtop guitar top plates, Journal of the Acoustical Society of America 150, 2 (2021) 1505–1513.
15. T. Duerinck, J. Segers, E. Skrodzka, G. Verberkmoes, M. Leman, W. Van Paepegem, M. Kersemans: Experimental comparison of various excitation and acquisition techniques for modal analysis of violins, Applied Acoustics 177 (2021) 107942.
16. L. Ausiello, L. Yule, G. Squicciarini, C. Barlow: Guitar soundboard measurements for repeatable acoustic performance manufacturing, in: Proceedings Reproduced Sound 2018, Bristol, UK, 27–29 November, 2018.
17. L. Ausiello, V. Hockey: Quantitative measurements to enhance performance of acoustic musical instruments and improve manufacturing, Acoustic Bulletin 47, 2 (2021) 30–45.
18. A. Farina: Simultaneous measurement of impulse response and distortion with a swept-sine technique, in: Proceedings of the AES 108 Convention, Paris, France, 19–22 February, Audio Engineering Society, 2000, pp. 1–24.
19. A. Farina: Advancements in impulse response measurements by sine sweeps, Proceedings of the AES 122 Convention, Vienna, Austria, 5–8 May, Audio Engineering Society, pp. 1–21.
20. S. Carcagno, R. Bucknall, J. Woodhouse, C. Fritz, C.J. Plack: Effect of back wood choice on the perceived quality of steel-string acoustic guitars, Journal of the Acoustical Society of America 144, 6 (2018) 3533–3547.
21. A. Brauchler, P. Ziegler, P. Eberhard: An entirely reverse-engineered finite element model of a classical guitar in comparison with experimental data, Journal of the Acoustical Society of America 149, 6 (2021) 4450–4462.
22. N. Giordano: Mechanical impedance of a piano soundboard, Journal of the Acoustical Society of America 103, 4 (1998) 2128–2133.
23. D. Brown, R. Allemang, A. Phillips: Forty years of use and abuse of impact testing: A practical guide to making good FRF measurements, in: J. De Clerck (Ed.), Experimental techniques, rotating machinery, and acoustics, vol. 8, Springer, Cham, 2015, pp. 221–241
24. M.J. Elejabarrieta, A. Ezcurra, C. Santamarıa: Evolution of the vibrational behaviour of a guitar soundboard along successive construction phases by means of the modal analysis technique, Journal of the Acoustical Society of America 108, 1 (2000) 369–378.
25. H. Mansour, G. Scavone, V. Freour: A comparison of vibration analysis techniques applied to the Persian setar, in: Proceedings of Acoustics, Nantes, France, 23–27 April, Société Française d'Acoustique, 2012, pp. 1743–1748.
26. W.G. Halvorsen, D.L. Brown: Impulse technique for structural frequency response testing, Sound and Vibration 63, 1 (1978) S81.
27. J. Curtin: Measuring violin sound radiation using an impact hammer, Journal of the Acoustical Society of America VSA Papers 22, 1 (2009) 186–209.
28. P. Guidorzi, L. Barbaresi, D. D'Orazio, M. Garai: Impulse responses measured with MLS or swept-sine signals applied to architectural acoustics: an in-depth analysis of the two methods and some case studies of measurements inside theaters, Energy Procedia 78 (2015) 1611–1616.
29. F. Policardi: Mls and sine-sweep technique comparison in room-acoustic measurements, Elektrotehniški Vestnik/Electrotechnical Review 78, 3 (2011) 91–95.
30. M. Garai, F. Morandi, D. D'Orazio, S. De Cesaris, L. Loreti: Acoustic measurements in eleven Italian opera houses: correlations between room criteria and considerations on the local evolution of a typology, Buildings and Environment 94 (2015) 900–912.
31. M. Pyrkosz, C. Van Karsen: Comparative modal tests of a violin, Experimental Techniques 37 (2013) 47–62.
32. L. Ausiello, G. Nicoletti: Fem simulations and experimental validation of frequency response prediction for acoustic soundboards, in: Proceedings of Reproduced Sound, Bristol, UK, 16–18 November, 2021.
33. N. Thiele: Loudspeakers in vented boxes: part 1, Journal of the Audio Engineering Society 19, 5 (1971) 382–392.
34. N. Thiele: Loudspeakers in vented boxes: part 2, Journal of the Audio Engineering Society 19, 6 (1971) 471–483.
35. R.H. Small: Vented-box loudspeaker systems – part 1: small-signal analysis, Journal of the Audio Engineering Society 21, 5 (1973) 363–372.
36. D. Ponteggia: Loudspeaker electrical impedance measurements methods: a brief review, in: International Conference on Noise and Vibration Engineering, Los Angeles, USA, 2006, pp. 1615–1626.
37. W. Klippel: Assessment of voice coil peak displacement Xmax, in: Proceedings of the AES 112 Convention, Dresden, Germany, 10–13 May, AES, 2002, pp. 307–324.
38. M. Dodd, W. Klippel, J. Oclee-Brown: Voice coil impedance as a function of frequency and displacement, in: Proceedings of the AES 117th Convention, San Francisco, CA, USA, 28–31 October, Audio Engineering Society, 2004, pp. 1–19.
39. M. Ducceschi, S. Duran, H. Tahvanainen, L. Ausiello: A method to estimate the rectangular orthotropic plate elastic constants using least-squares and Chladni patterns, Applied Acoustics 220 (2024) 109949.
40. M. Ducceschi, C. Touzé, S. Bilbao, C.J. Webb: Nonlinear dynamics of rectangular plates: Investigation of modal interaction in free and forced vibrations, Acta Mechanica 225, 1 (2014) 213–232.
41. A. Prato, A. Schiavi, F. Casassa: A modal approach for reverberation time measurements in non-diffuse sound field, in: 23nd International Congress of Sound and Vibration (ICSV), Athens, Greece, 10–14 July, 2016.
42. J. Lazar, G.S. Kubota: Analysis of a vented-box loudspeaker system via the impedance function, in: 147th Audio Engineering Society Convention 2019, New York, New York, USA, 16–19 October, 2019.
43. R. Magalotti, K. Bugaj, A. Said: Assessing the acoustic load on a loudspeaker driver through electrical impedance measurements, in: 4th International Conference on Acoustics & Sound Reinforcement (ASR 2024), Le Mans, France, 22–26 January, 2024.
44. K.G. McConnell: Vibration testing: theory and practice, John Wiley & Sons, Hoboken, New Jersey, 1995.
45. P. Varoto, L. de Oliveira: Interaction between a vibration exciter and the structure under test, Sound and Vibration 36 (2002) 20–26.
46. G. Caldersmith: Guitar as a reflex enclosure, Journal of the Acoustical Society of America 63, 5 (1978) 1566–1575.
47. B. Katz: Mastering audio: the art and the science, Elsevier/Focal Press, Waltham, Massachusetts, 2007.

Cite this article as: Ausiello L. Ducceschi M. Duran S. & Morrison B. 2024. Affordable wide-band measurement ecosystem for musical acoustics based on electro-dynamic transducers. Acta Acustica, **8**, 53.